Simple, Helical Peptoid Analogs of Lung Surfactant Protein B

Shannon L. Seurynck, James A. Patch,
and Annelise E. Barron*
Department of Chemical and Biological Engineering
Northwestern University
2145 Sheridan Road
Evanston, Illinois 60208

Summary

The helical, amphipathic surfactant protein, SP-B, is a critical element of pulmonary surfactant and hence is an important therapeutic molecule. However, it is difficult to isolate from natural sources in high purity. We have created and studied three different, nonnatural analogs of a bioactive SP-B fragment (SP-B$_{1-25}$), using oligo-*N*-substituted glycines (peptoids) with simple, repetitive sequences designed to favor the formation of amphiphilic helices. For comparison, a peptide with a similar repetitive sequence previously shown to be a good SP mimic was also studied, along with SP-B$_{1-25}$ itself. Surface pressure-area isotherms, surfactant film phase morphology, and dynamic adsorption behavior all indicate that the peptoids are promising mimics of SP-B$_{1-25}$. The extent of biomimicry appears to correlate with peptoid helicity and lipophilicity. These biostable oligomers could serve in a synthetic surfactant replacement to treat respiratory distress syndrome.

Introduction

Exogenous surfactant replacement therapy is commonly used to treat respiratory distress syndrome (RDS) in prematurely born infants lacking surfactant and has greatly decreased the mortality rate [1]. For treatment, an animal-derived lung surfactant (LS) replacement is instilled into the alveolar network via an intratracheal tube. Within a few days of treatment, functional surfactant begins to be secreted into alveolar spaces as the lungs mature. However, while the infant continues to rely on the exogenous material to enable breathing, critical surfactant-associated lipids and proteins can either be recycled via tubular myelin or cleared from the alveolus by various mechanisms, including phagocytosis by inflammatory cells and degradation by lytic enzymes [2–5]. Hence, the delivery of repeated doses of an LS replacement over the course of 3–5 days is often necessary. Some drawbacks to this treatment are that animal-derived replacements are expensive and carry the risk of viral transmission [6]. For these and other reasons, there is currently a great deal of interest in the development of a synthetic, biomimetic LS replacement that can be used for the effective, safe, and lower-cost treatment of RDS [7–9]. The necessary biophysical properties for a functional surfactant replacement include the following: (1) rapid adsorption to the air/water interface, (2) the ability to reach near-zero surface tension upon film compression, and (3) the ability to respread upon multiple compressions and expansions of surface area with minimal loss of surfactant into the subphase [10]. LS is composed of ~90% lipids and ~10% surfactant proteins [5, 11–15]. The hydrophobic surfactant proteins, SP-B and SP-C, in particular are essential to the proper biophysical function of LS for breathing and are thought to be involved in the organization and fluidization of the lipid film [10].

Films of the main lipid component of LS, dipalmitoyl phosphatidylcholine (DPPC), can reach near-zero surface tension upon compression in vitro; however, this molecule is slow to adsorb to the interface and exhibits poor respreadability [10]. With the addition of palmitoyl-oleoyl phosphatidylglycerol (POPG) and/or palmitic acid (PA), there is an increased rate of surfactant adsorption and better respreadability than with DPPC alone [16]. However, these lipid mixtures do not reach sufficiently low surface tensions [16]. The addition of small amounts of SP-B and/or SP-C to the lipid film has been shown to greatly accelerate the kinetics of adsorption, decrease the surface tension upon compression to nearly zero, and induce good respreadability [1, 10, 17, 18]. However, due to relative scarcity, as well as the hydrophobic and surface-active nature of these proteins, it is difficult and costly to isolate them from natural sources in high purity [19]. Here, we report the development of novel, nonnatural, peptidomimetic replacements for SP-B.

SP-B is a 79 amino acid amphipathic protein with a predominantly helical structure [20–22]. It contains seven cysteine residues that form three intramolecular disulfide bonds and, in its natural form, is homodimerized through an additional, intermolecular disulfide bond [23]. Although the specific mechanisms by which SP-B interacts with the lipid film to enable breathing are not yet well understood, some interesting hypotheses have been put forward [24]. Recently, there has been interest in the creation of synthetic mimics of SP-B that can serve as effective additives to a biomimetic LS replacement. Chemically synthesizing the entire, dimerized SP-B protein is a daunting task, so small fragments of the SP-B monomer have been investigated for their ability to mimic the surface activity of the natural protein [25–28]. A small, helical, facially amphipathic segment from the N-terminus, SP-B$_{1-25}$ (Table 1), has been shown to retain much of the surfactant function of the full-length synthetic peptide, both in vitro and in vivo [26–30]. Structural studies of SP-B$_{1-25}$ by FTIR [31] and of SP-B$_{11-25}$ by 2D-NMR [32] reveal that residues 8–22 are mainly helical, while residues 1–7 form a hydrophobic, flexible β strand, potentially for insertion into the lipid film. These studies also show that the α-helical domain is facially amphipathic, with cationic and nonpolar faces [31, 32]. A simplified, de novo-designed peptide mimic of SP-B$_{1-25}$ called "KL$_4$," a 21-mer, which is locally amphipathic (Table 1), composed of only leucine and lysine, also has been investigated for use in a synthetic LS replacement [33]. Despite its

*Correspondence: a-barron@northwestern.edu

Table 1. SP-B Mimic Sequences, Molar Masses, and Crude Yields

Oligomer	Monomer Sequence (Amino to Carboxy)[a]	Molar Mass (Da) Calculated: Found	Crude Yield (%)[b]	% HPLC Elution
SP-B$_{1-25}$ (C8→A, C11→A)	FPIPLPYAWLARALIKRIQAMIPKG	2865.55: 2865.3	56	55.9
KL$_4$	KLLLLKLLLLKLLLLKLLLLK	2469.4: 2469.7	60	53.4
Peptoid **1**	Nspe-Nspe-(NLys-Nspe-Nspe)$_5$	2592.4: 2592.5	66	57.5
Peptoid **2**	Nssb-Nspe-(NLys-Nssb-Nspe)$_5$	2304.1: 2303.5	76	45.5
Peptoid **3**	Nssb-Nssb-(NLys-Nssb-Nssb)$_5$	2015.8: 2015.7	62	38.9

[a] Cationic side chains are underlined.
[b] As estimated by analytical reversed-phase HPLC of crude product. All compounds were purified to >97% homogeneity before analysis and characterization.

simplicity of sequence, the KL$_4$ peptide, in combination with lipids, has been shown to have good surface activity in vitro as well as useful in vivo efficacy for the treatment of RDS in an animal model [30, 34–38].

Since peptides have a very short half-life in vivo and are relatively expensive to synthesize and purify, there is great interest in developing nonnatural, sequence-specific oligomers as protein mimics for therapeutic purposes [39–41]. We have been working with a family of peptide mimics called "peptoids" (oligo-N-substituted glycines), which have the same backbone structure as peptides but have their side chains appended to the amide nitrogen rather than the α-carbon [42, 43]. Diverse peptoid sequences up to ∼40 monomers in length can be synthesized in good yield on a standard, automated peptide synthesizer, using a facile and relatively low-cost "submonomer" approach [43–47]. Peptoids are protease resistant due to the nonnatural placement of the side chain [45], and although the N-substituted glycine backbone is achiral, stable helical secondary structure can be induced sterically through the inclusion of chiral side chains [48, 49]. NMR structural studies of a peptoid pentamer with bulky, aromatic, α-chiral side chains (i.e., with chirality introduced at the α-carbon) revealed a polyproline type I-like helical structure with cis-amide bonds in the backbone, a helical pitch of ∼6 Å, and roughly three monomers per turn [50]. X-ray crystallographic studies later showed that a peptoid pentamer with α-chiral aliphatic side chains forms the same type of helix with a slightly longer helical pitch (∼6.7 Å) [51]. Peptoid helices in both organic and aqueous solution are stable and robust, showing no significant denaturation at temperatures of up to 75°C, even in the presence of 8 M urea in the case of water-soluble peptoids [46]. Studies of certain heterooligomeric peptoids revealed that helices are stabilized by the inclusion of (1) at least one-half α-chiral side chains, (2) an aromatic, α-chiral face, and (3) an aromatic, α-chiral side chain at the C terminus if the peptoid has a carboxamide tail [52]. Previous studies have demonstrated that various sequence-specific peptoids from 3 to 22 monomers in length exhibit a variety of interesting biological activities [47, 53, 54].

In this study, we have designed and synthesized three simple peptoid oligomers meant to mimic the N-terminal region of SP-B. The designs for these oligomers are based on the prominent molecular features of SP-B$_{1-25}$, including its helicity, facial amphipathicity, and overall lipophilicity, as well as the relative simplicity of the KL$_4$ sequence. The three peptoids we designed are each 17-mers and exhibit varying extents of helicity and lipophilicity, as determined by CD studies in organic, aqueous, and liposome environments and RP-HPLC, respectively. The surface activities of these peptoids, when combined with a lipid mixture that has been shown to mimic well the nonprotein fraction of LS [55], was investigated and compared to that of an SP-B$_{1-25}$ peptide mimic and the KL$_4$ peptide using a Langmuir-Wilhelmy surface balance to obtain surface pressure-area isotherms, imaging by fluorescence microscopy to examine film morphology, and a pulsating bubble surfactometer to study surfactant adsorption dynamics. The results reveal that these peptoids with relatively simple sequences show good mimicry of the essential surface-active behaviors of the SP-B$_{1-25}$ peptide, with mostly subtle but, in some cases, dramatic differences in activity arising from their different structures. The surface-active behaviors of these simple peptoids also seem to correlate with their extent of helicity and overall lipophilicity, with the most helical and lipophlic molecule best mimicking the SP-B$_{1-25}$ peptide.

Results and Discussion

Design of Mimics

SP-B is known to be essential to proper respiratory function and hence must be included or replaced with a functional mimic in an exogenous pulmonary surfactant replacement for the treatment of respiratory distress syndrome. Although it is a relatively small protein at 79 residues, the complexity of its structure, in particular its multiple disulfide bonds, makes it challenging to synthesize chemically and then obtain in a properly folded form. Therefore, various segments of SP-B in combination with surface-active lipids have been investigated for their in vitro surface activity as well as their in vivo efficacy in an animal model of RDS [25–28]. A segment from the N terminus, SP-B$_{1-25}$, has been extensively investigated and shows promise as a simple mimic of the biophysical function of the entire protein both in vitro and in vivo [26, 27, 29, 30]. Hence, it is this bioactive peptide that we have sought to mimic with a sequence-specific, folded peptoid oligomer. For comparison with the peptoid mimics, we have synthesized a 25 residue peptide based on the sequence of SP-B$_{1-25}$, with cysteine-to-alanine substitutions at positions 8 and 11 to prevent the formation of unwanted
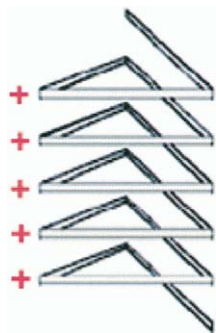
Figure 1. The Design Scheme for Amphiphilic Peptoid Helices to Mimic SP-B$_{1-25}$ and KL$_4$

The peptoid helix is designed to have three-fold periodicity with one cationic face (red +) and two hydrophobic faces (black).

disulfide linkages (Table 1). This modified peptide has previously been shown to retain the function of the original, unmodified sequence [27]. For further comparison, we synthesized the simple KL$_4$ peptide that has also previously been shown to be a good SP mimic [30, 33–38]. After purification, the final purities of the peptides were confirmed to be >97% by RP-HPLC, and the molar masses were confirmed to be correct at 2865 Da for SP-B$_{1-25}$ and 2470 Da for KL$_4$ by ESI mass spectrometry.

Peptoid-based SP-B mimics were designed to comprise three main structural features of the N-terminal protein segment that are thought to be important to its function: (1) overall helicity, (2) overall lipophilicity, and (3) an amphiphilic patterning of cationic and nonpolar faces on the helix, i.e., facial amphipathicity (Figure 1). In order to maintain a stable, helical secondary structure, we included the following sequence aspects in two of the peptoids (1 and 2, Table 1): (1) the inclusion of more than two-thirds α-chiral side chains, (2) the patterning of at least one α-chiral, aromatic face on the peptoid helix, and (3) two α-chiral side chains at the C terminus to minimize helix fraying [52]. The third peptoid (3) was designed to be the most biomimetic in its side-chain chemistry and therefore included no aromatic side chains, as none are found in the helical region of SP-B$_{1-25}$ (Table 1). Based on the results of previous structural studies, we estimated that the proper, most biomimetic length for the peptoids would be about 19 monomers, assuming a helical rise of $\sim$3 monomers per turn and a pitch of $\sim$6 Å [50]. However, since all of the peptoid mimics include one-third achiral side chains (the lysine-like NLys monomers), we anticipated a slight "loosening" and lengthening of the helical structure relative to the peptoids for which the structures were solved, so the SP-B mimics were designed to be 17 monomers in length. Figure 1 shows a schematic of the design for the peptoid mimics. In order to create a cationic face on the peptoid helix, as observed in SP-B$_{1-25}$, we have placed an NLys side chain every third monomer. The peptoid mimics each have five cationic groups, while SP-B$_{1-25}$ has four and KL$_4$ has five (Table 1). The nonpolar face of the helix was made by patterning hydrophobic side chains, in-

cluding N-(S)-phenylethylamine (Nspe) and/or N-(S)-sec-butylamine (Nssb), with three-fold periodicity in the remaining two-thirds of the peptoid sequence (side chain structures are shown in Table 2). For peptoid 1, the hydrophobic side chains are all α-chiral and aromatic (Nspe). Based on our prior studies [46, 52], we expected this sequence patterning to produce a peptoid helix with excellent structural stability. We have also designed a peptoid (2) that is somewhat more biomimetic in its sequence design, including an α-chiral, aliphatic, isoleucine-like side chain, Nssb, every third monomer, while still maintaining one aromatic face to help stabilize the peptoid helix [52]. Finally, we synthesized a peptoid oligomer (3) with entirely aliphatic chemistry for the hydrophobic groups, with two-thirds Nssb monomers and a cationic NLys in every third sequence position. This peptoid is the closest structural analog of the KL$_4$ peptide.
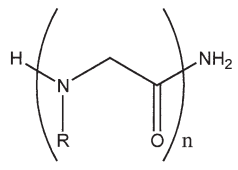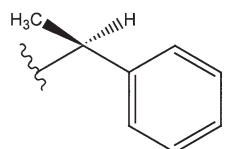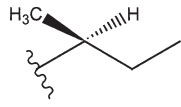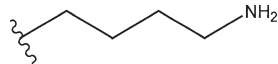
The three peptoids were synthesized by the submonomer method [43] and were obtained in good yield (Table 1). The final purities of the compounds were confirmed to be >97% by RP-HPLC, and molar masses were confirmed by ESI to correspond with the desired molecular structures (1, 2592 Da; 2, 2304 Da; 3, 2016 Da). Due to the different side-chain chemistries employed, the lipophilicities of these molecules differed significantly, as indicated by RP-HPLC elution times (Table 1), with 1 > 2 > 3.

CD Spectroscopy in Water and in Liposomes

The solution conformations of these SP mimics were studied by CD spectroscopy. Figure 2A shows a comparison of the CD spectra obtained for the SP-B$_{1-25}$ peptide and for peptoids 1, 2, and 3 in water at room temperature. We find that the SP-B peptide fragment has a spectrum that is characteristic of an unstructured, random-coil conformation under these conditions. However, as expected, both 1 and 2 show α-helix-like spectral features (two minima at λ $\sim$202 nm and $\sim$218 nm and a maximum at λ $\sim$192 nm) [48, 52], which were previously shown to correspond to a polyproline type I-like helical structure for peptoids comprising a significant fraction of Nspe side chains [48–50, 52]. The spectrum of 1 shows more intense helical features than that of 2, as expected due to the higher Nspe content of 1 [52]. The CD spectrum of 3 is that typically seen for a peptoid oligomer with a random-coil conformation [54].

In order to characterize the conformations of these SP-B mimics in a lipid environment similar to that of LS, CD was also performed in an aqueous solution of LS-mimetic liposomes, with an overall lipid concentration of 1 mM (Figure 2B). We chose a lipid formulation that has previously been shown to be a good mimic of the nonprotein fraction of LS, in particular DPPC:POPG:PA 68:22:9 by weight [55]. In liposomes, all four oligomers exhibit spectra characteristic of helices. However, as expected, the spectrum for 3 is similar to that typically seen for a polyproline type-I helix, with a positive CD band at $\sim$208 nm [51]. This type of spectrum has previously been observed for helical peptoids comprising chiral, aliphatic side chains [51, 52]. The spectra of the SP-B$_{1-25}$ peptide, 1, and 2 all show

Table 2. *N*-Substituted Glycine Side-Chain Structures

	N-Substituted Glycine Oligomer or Peptoid

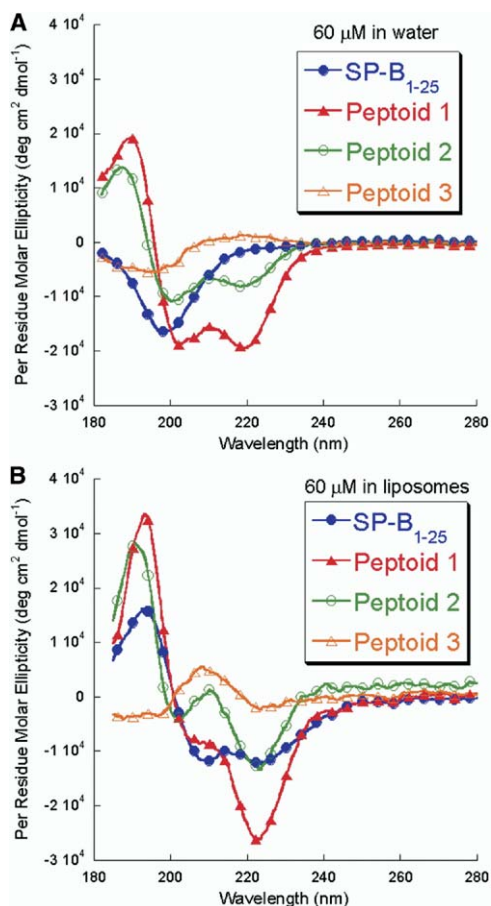| R = Side Chain	Designator
	*N*spe = (S)-*N*-(1-phenylethyl)glycine
	*N*ssb = (S)-*N*-(2-butyl)glycine
	*N*Lys = *N*-(4-aminobutyl)glycine

Figure 2. CD Spectra

CD spectra for SP-B$_{1-25}$ (blue, filled circles), **1** (red, filled triangles), **2** (green, open circles), and **3** (orange, open triangles) in water (A) and liposomes (B).

α-helix-like features typically associated with helical peptides and peptoids of these classes. Interestingly and perhaps not unexpectedly, the CD spectrum of **2** appears to be an average of that of **1** and **3** in this lipid environment, most likely due to the inclusion of both aromatic and aliphatic side chains. For all compounds, the spectra in liposomes are substantially more intense and are shifted toward higher wavelengths, in comparison to those observed in water, implying greater helicity of all of these molecules in a lipid film. In addition, the spectral minimum at $\sim$220 nm for both **1** and **2** is more intense than that at $\sim$205 nm, corresponding to more stable helical structure for peptoids [49, 52]. This spectral feature is not observed in water, indicating that the lipid environment induces increased helical stability for these amphiphilic peptides. In both aqueous and lipophilic environments, **1** and **2** appear to be substantially more helical than SP-B$_{1-25}$; previous studies have shown that peptoid helices can be formed at a shorter length than peptide helices due to the predominantly steric stabilization of peptoid folding [46, 48, 49]. Similar trends for all of the peptides and peptoids studied were observed when CD spectra were collected in methanol solution (data not shown). Previous CD studies of KL$_4$ have shown that it is α helical in a lipid film [56].

Langmuir-Wilhelmy Surface Balance Studies

Langmuir-Wilhelmy surface balance (LWSB)-derived surface pressure (Π)-area (A) isotherms for good LS replacements are expected to exhibit an early lift-off (i.e., an increase in surface pressure at a relatively large area per molecule [>100 mN/m], indicating rapid surfactant adsorption to the air-water interface), a high film collapse pressure (near 70 mN/m, a value that corresponds to near-zero surface tension), and a kink or plateau in the isotherm at a surface pressure of $\sim$40-50 mN/m (corresponding to a phase transition in the lipid
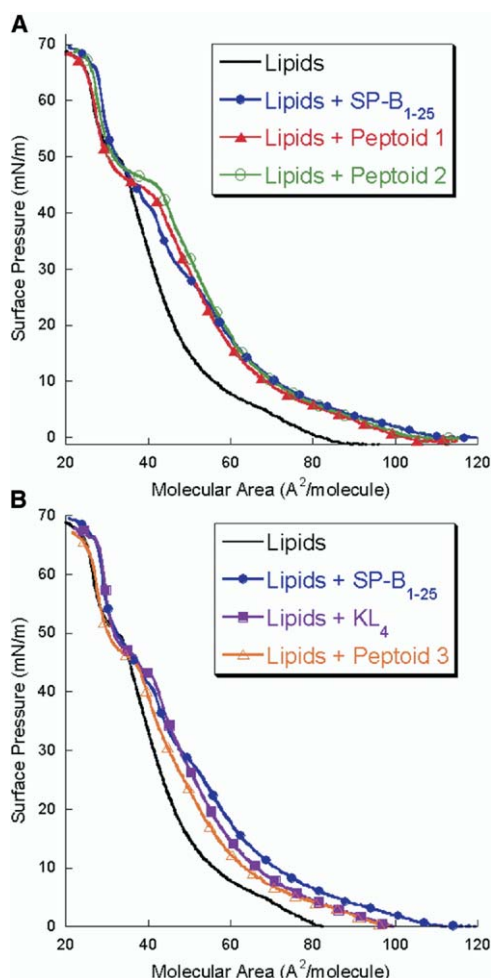
Figure 3. Surface Pressure-Molecular Area Isotherms Collected on a LWSB

(A) Π-A isotherms for lipids alone (black), lipids + 2.16 mol% SP-B$_{1-25}$ (blue, filled circles), lipids + 2.16 mol% **1** (red, filled triangles), and lipids + 2.16 mol% **2** (green, open circles) on buffer at 25°C with a barrier speed of 30 mm/min.
(B) Π-A isotherms for lipids alone (black), lipids + 2.16 mol% SP-B$_{1-25}$ (blue, filled circles), lipids + 2.16 mol% KL$_4$ (purple, filled squares), and lipids + 2.16 mol% **3** (orange, open triangles) on buffer at 25°C with a barrier speed of 30 mm/min.

film, and/or to the "squeeze-out" of molecules other than DPPC from the monolayer) [57]. We collected and compared Π-A isotherms for the lipid mixture by itself (DPPC:POPG:PA 68:22:9 by weight), lipids with the addition of 2.16 mol% (10 wt%) SP-B$_{1-25}$, lipids with 2.16 mol% KL$_4$, and lipids with 2.16 mol% of either peptoid **1**, **2**, or **3**, at both 25°C and 37°C. We chose to add 10 wt% SP-B$_{1-25}$ based on previous work by other groups who have studied SP-B at this concentration in an attempt to mimic the overall protein content of LS [25, 58, 59]. We show the Π-A isotherms collected at 25°C; similar trends were observed at 37°C (see Supplemental Data). The isotherms for the lipid mixture and the lipid/SP-B$_{1-25}$ mixture are plotted in both Figures 3A and 3B to facilitate comparisons. Isotherms for peptoids **1** and **2** are plotted in Figure 3A, while those for KL$_4$ and **3** are shown in Figure 3B.

Examination of Figure 3A shows that the lipid mixture exhibits lift-off at a molecular area of ~87 Å^2/molecule. As expected, the lipid/SP-B$_{1-25}$ surfactant mixture shows a substantially earlier lift-off [25, 27] at ~110 Å^2/molecule and also has an incipient plateau in the isotherm at ~50 mN/m (a more dramatic plateau is seen at 37°C). Figure 3B shows that the lipid/KL$_4$ mixture has a level of surface activity intermediate between that of the lipid mixture and the lipid/SP-B$_{1-25}$ mixture, with lift-off at ~100 Å^2/molecule and an incipient plateau at ~45 mN/m. When either peptoid **1** or **2** is added to the lipids, we observe isotherms that are dramatically different than what is seen for lipids alone and much more similar to what is observed for the lipid/SP-B$_{1-25}$ mixture, with lift-off at ~105 mN/m and plateau in the isotherm at ~45 mN/m (Figure 3A). Peptoid **3**, on the other hand, has a Π-A isotherm that is very similar to that of KL$_4$ (Figure 3B).

At this point, it behooves us to note that the fundamental phase behavior of LS on a Langmuir trough, as it affects the shape of the Π-A isotherms, is not yet deeply understood; hence, it is not known for certain to what extent the small differences in the isotherms for the different peptides and peptoids might affect their in vivo efficacy as LS replacements (we intend to investigate this). This being said, we do observe some interesting trends, from which we believe we can infer the likely relative bioactivities of these different SP-B mimics. For both lipid/**1** and lipid/**2** films, there is a very pronounced plateau in the isotherm (Figure 3A), which is much more dramatic than that seen for either of the peptides and more similar to that observed for natural LS [57, 60]. We believe that this may be due to the greater stability of the helical structures of peptoids **1** and **2** as compared to SP-B$_{1-25}$. On the other hand, it can be seen that KL$_4$ and peptoid **3** both show a kink in their isotherm but not a defined plateau. Peptoid **3** has all aliphatic side chains and hence a less stable helical structure [51], which may be why it is a better mimic of KL$_4$ than of SP-B$_{1-25}$.

It has been shown by infrared reflection-absorption spectroscopic studies on a Langmuir trough that both SP-B$_{1-25}$ and KL$_4$ can adopt extended β-type conformations in the lipid film at increased surface pressures [61, 62]. It is unknown whether this α-helix-to-β-sheet transformation takes place in the natural, dimerized SP-B protein. Due to the lack of hydrogen-bond donors along the *N*-substituted glycine backbone, peptoids are unable to form β sheets. This may allow the peptoid oligomers to better mimic the biophysical function of the natural protein at high surface pressures, as compared to these peptide mimics.

In order to determine the respreadability of the films, the barriers were first compressed to near collapse (as shown in Figure 3 at A ~20 Å^2/molecule), then expanded fully, and compressed again. By doing this, we are able to compare the relative respreadabilities of these surfactant formulations based on determinations of the lift-off areas for the first and second compressions. From this analysis, we found that the respreadabilities of films containing the peptoids **1**, **2**, and **3** were comparable to those of the peptides and significantly better than that of the lipids in the absence of
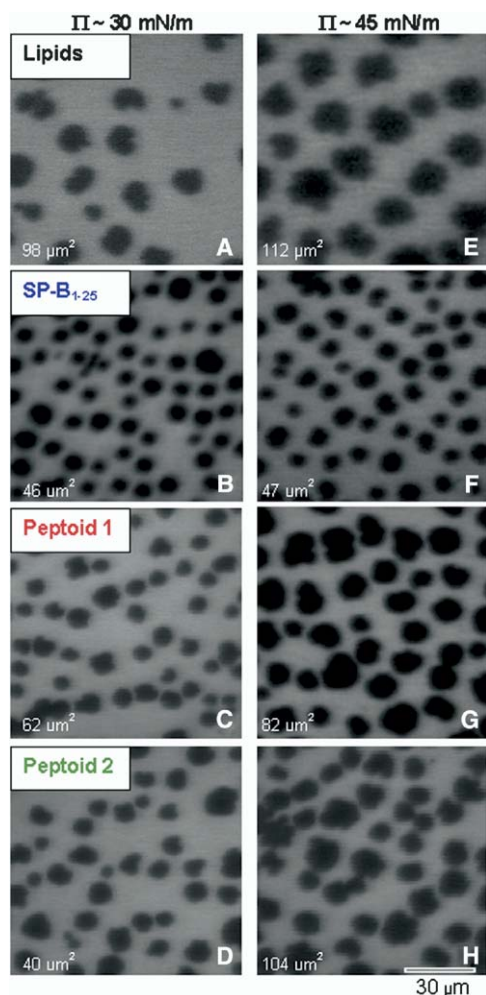
Figure 4. FM Images of Surfactant Film Phase Behavior on a Langmuir Trough

FM images for lipids alone ([A] and [E]), lipids + 2.16 mol% SP-B$_{1-25}$ ([B] and [F]), lipids + 2.16 mol% **1** ([C] and [G]), and lipids + 2.16 mol% **2** ([D] and [H]) on buffer at 37°C collected with a barrier speed of 2–10 mm/min. Images shown for Π ∼30 mN/m ([A]–[D]) and Π ∼45 mN/m ([E]–[H]). Average domain area is shown in lower left corner.

these helical, amphipathic spreading agents (data not shown).

Fluorescence Microscopy Imaging of Surfactant Film Morphology

Fluorescence microscopy (FM) imaging, in conjunction with the LWSB, was used to investigate the surface phase morphology of lipid, lipid/peptide, and lipid/peptoid films at the air-water interface. This experimental approach was previously used to study the surface-active behavior of SP-B$_{1-25}$ on an instrument similar to ours [25, 58, 59, 63]. The samples were spiked with a Texas red-conjugated lipid (1 mol%) that preferentially resides in the more expanded surface phase. Therefore, in the FM images shown in Figure 4, the lighter regions correspond to the more expanded phase, while the darker regions correspond to the more condensed phase. FM images obtained at 37°C for lipids (panels A and E), lipid/SP-B$_{1-25}$ (B and F), lipid/**1** (C and G), and lipid/**2** (D and H) at surface pressures of ∼30 mN/m (A–D) and ∼45 mN/m (E and F) are shown in Figure 4. At Π ∼30 mN/m, the lipid film exhibits condensed-phase domains that are relatively large (averaging ∼98 μm^2 in area) and rather spread out (Figure 4A). With the addition of the SP-B$_{1-25}$ peptide to the lipid film at the same surface pressure, a significant decrease in the domain size is observed (to ∼46 μm^2), as well as a coexistence of small and medium condensed-phase domains and a more closely packed domain arrangement than seen for lipids alone (Figure 4B). Similar results were found for natural SP-B in a DPPC film, with a reduction in domain size and increase in the number of domains [64]. FM images and trends similar to this are observed when KL$_4$ is present in the lipid film (data not shown). FM imaging of both lipid/**1** and lipid/**2** mixtures at ∼30 mN/m reveals an essentially similar coexistence of small- and medium-sized domains as seen for SP-B$_{1-25}$, with a packing arrangement that appears to be intermediate between that of lipids alone and lipid/SP-B$_{1-25}$, though with more similarity of the film morphology to the peptide-spiked film (Figures 4C and 4D). The average domain sizes for **1** (∼62 μm^2) and **2** (∼40 μm^2) at this surface pressure are much more similar to that found for SP-B$_{1-25}$ (∼46 μm^2) than for lipids alone (∼98 μm^2). This difference in condensed-phase domain size and packing is also observed at 45 mN/m, with lipids alone exhibiting large, widely spaced domains averaging ∼112 μm^2 (Figure 4E), and the lipid/SP-B$_{1-25}$ film showing both small- and medium-sized domains, averaging ∼47 μm^2, that are more closely packed (Figure 4F). At 45 mN/m, lipid/**1** and lipid/**2** films show a coexistence of medium-sized and large domains, with an average size more similar to lipids alone than to the domains in the lipid/SP-B$_{1-25}$ film (∼82 μm^2 for **1** and ∼104 μm^2 for **2**), though with packing arrangements resembling the lipid/SP-B$_{1-25}$ film (Figures 4G and 4H). Recall, however, that SP-B$_{1-25}$ has been shown to make a transformation from α helix to β sheet at high surface pressures, such as those that we are investigating here [61, 62]. Hence, it is unknown whether SP-B$_{1-25}$-containing films exhibit phase morphology similar to what would be seen for the natural SP-B dimer at this higher surface pressure. This being said, SP-B$_{1-25}$ does show promising in vivo activity [29, 65, 66]. It may be that the ability of an SP-B mimic to maintain a small average condensed-domain size upon compression, which is expected to increase the fluidity of the surfactant film, correlates with in vivo activity. If this is the case, these FM images may indicate that we still have some more work to do in optimizing the design of the peptoid-based SP-B mimics, so that upon compression they yield smaller condensed domains. Trends for lipid/**3** films were essentially similar to those of **1** and **2** (data not shown).

Pulsating Bubble Surfactometry

A pulsating bubble surfactometer (PBS) was used to characterize and compare the dynamic surface activities of lipids alone as well as the peptides and peptoids in a lipid film. In this technique, a small air bubble is
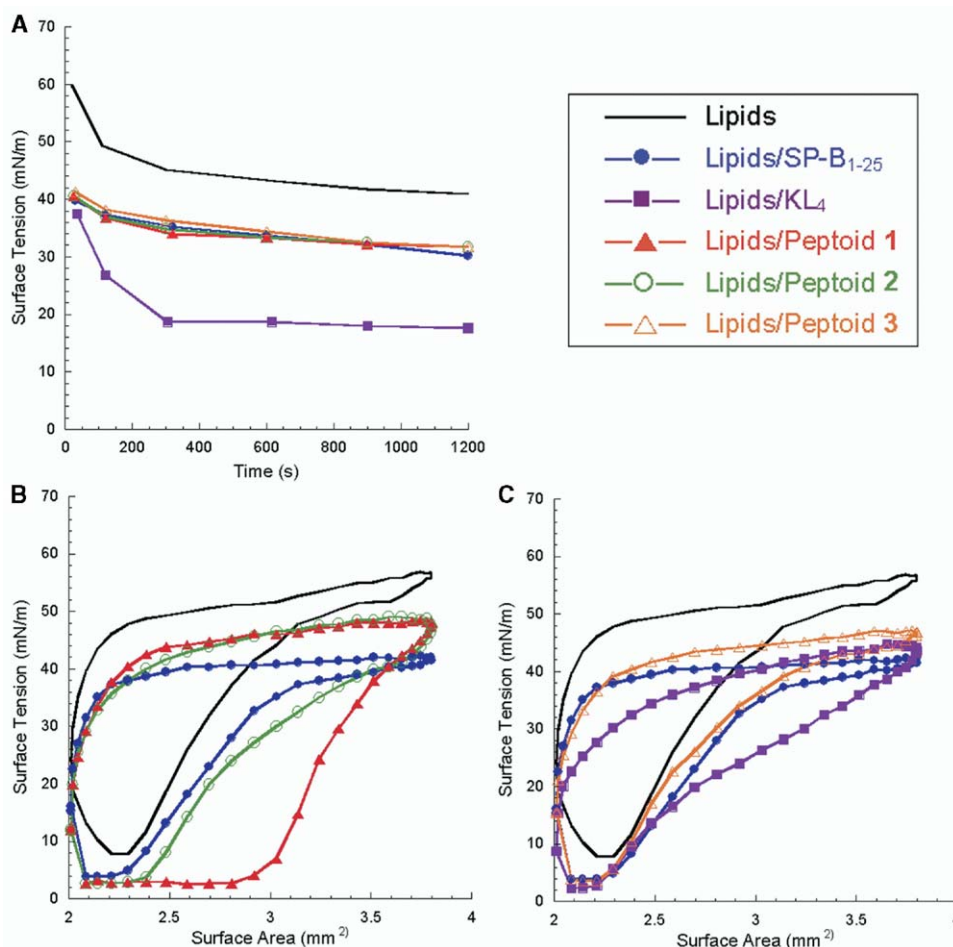
Figure 5. Static and Dynamic Adsorption Data Collected on a PBS

Static (A) and dynamic ([B] and [C]) adsorption data for lipids alone (black), lipids + 2.16 mol% SP-B$_{1-25}$ (blue, filled circles), lipids + 2.16 mol% KL$_4$ (purple, filled squares), lipids + 2.16 mol% **1** (red, filled triangles), lipids + 2.16 mol% **2** (green, open circles), and lipids + 2.16 mol% **3** (orange, open triangles) in buffer at 37°C with a pulsation rate of 20 cycles/min.

formed within the surfactant solution, and the pressure difference across the air-water interface is measured as a function of either time (for a static bubble) or bubble surface area (for a pulsating bubble) [67]. Surface tension is calculated using the Laplace equation for a sphere. Static adsorption data were collected at the minimum bubble radius (0.4 mm) over 20 min, and dynamic data were collected as the bubble surface area was pulsed at 20 cycles per minute, with a minimum bubble radius of 0.4 mm and a maximum radius of 0.55 mm.

Static adsorption data were collected for lipids alone, lipids/SP-B$_{1-25}$, lipids/KL$_4$, and lipids/peptoid **1**, **2**, or **3** over 20 min at 37°C (Figure 5A). Note that natural LS is typically seen to attain essentially complete (quasi-static equilibrium) adsorption to the bubble interface in under 1 min, with an equilibrium surface tension of 20–25 mN/m [68]. The equilibrium surface tension attained by lipids alone (after 20 min) is relatively high at ∼40 mN/m. With added SP-B$_{1-25}$, the surface tension rapidly decreases to ∼40 mN/m in only 2 min and then slowly decreases to an equilibrium surface tension of ∼30 mN/m. The lipid/KL$_4$ mixture adsorbs to the interface very rapidly and reaches a substantially lower equilibrium surface tension of ∼20 mN/m. On the other hand, the addition of peptoid **1**, **2**, or **3** to the lipids has an effect very similar to that of SP-B$_{1-25}$, with an immediate decrease of surface tension to ∼40 mN/m followed by a gradual decrease to an equilibrium surface tension of ∼30 mN/m. All of the mimics facilitate greatly improved adsorption kinetics over lipids alone, reaching equilibrium surface tensions of ∼30 mN/m or less versus ∼40 mN/m for lipids alone. It is generally thought that the ability of a biomimetic LS formulation to rapidly reach a very low equilibrium surface tension correlates with in vivo efficacy; hence, by this measure KL$_4$ appears to be very promising.

Dynamic adsorption data were collected on the PBS for the same set of samples at 37°C and with a pulsation rate of 20 cycles/min; the resulting hysteresis loops (interfacial area versus surface tension) are shown in Figures 5B and 5C. Note that typical PBS results for natural LS show a hysteresis loop with a maximum surface tension of ∼35 mN/m, a minimum surface tension near zero, and very rapid adsorption to the interface upon bubble compression, the latter manifested as a

steep slope in the data loop at high surface areas as well as a large overall loop hysteresis [68]. As in Figure 3, we have divided the data onto two separate plots for greater clarity. Data loops for lipids alone and lipid/SP-B$_{1-25}$ are plotted in both Figures 5B and 5C to facilitate close comparisons. Loops for lipid/1 and lipid/2 films are plotted in Figure 5B, while loops for lipid/KL$_4$ and lipid/3 films are plotted in Figure 5C. The data loop for lipids alone exhibits a relatively small extent of hysteresis, especially at high surface areas, and reaches a relatively high maximum surface tension of $\sim$57 mN/m and a minimum surface tension of $\sim$7 mN/m. Upon the addition of SP-B$_{1-25}$ to the lipid mixture, we observe a significant decrease in both the maximum and minimum surface tensions reached, to $\sim$42 mN/m and $\sim$4 mN/m, respectively. The extent of loop hysteresis, however, is not much changed. The lipid/KL$_4$ mixture exhibits a hysteresis loop that is in many ways similar to that of SP-B$_{1-25}$ but with some distinct features (Figure 5C): a lower minimum surface tension of $\sim$2 mN/m, a slightly higher maximum surface tension of $\sim$44 mN/m, and a significant increase in loop hysteresis at medium-to-high surface areas in comparison to both lipids alone and the SP-B$_{1-25}$-spiked film. These minimum and maximum surface tensions are comparable to those previously found for lipid/KL$_4$ films [36].

With the addition of either peptoid 1 or 2 (Figure 5B), a minimum surface tension a bit lower than that of the lipid/SP-B$_{1-25}$ mixture is observed ($\sim$4 mN/m); however, the maximum surface tension is intermediate between that observed for lipids alone and for the lipid/SP-B$_{1-25}$ mixture ($\sim$49 mN/m). Interestingly, the data loops for peptoids 1 and 2 show a substantial increase in hysteresis compared to the loop for SP-B$_{1-25}$, indicating that the peptoid mimics of SP-B may actually be mimicking some features of natural LS better than the peptide segment (this may also be the case for KL$_4$). This increased loop hysteresis is particularly dramatic for peptoid 1, the most helical and lipophilic peptoid mimic (note that 1 is more helical in a lipid environment than the SP-B$_{1-25}$ peptide segment [Figure 2B] and has a molecular lipophilicity similar to SP-B$_{1-25}$ [Table 1]). The hysteresis loop for the lipid/1 mixture is the most similar in shape to that observed for natural LS [68] of all the formulations we studied here. It differs from natural LS data loops primarily in the higher value of the maximum surface tension it exhibits ($\sim$49 mN/m versus $\sim$35 mN/m for natural LS). Finally, the dynamic surface-active behavior of peptoid 3, shown in Figure 5C, looks very similar to that of SP-B$_{1-25}$ but with a slightly higher maximum surface tension.

Conclusions

We have used four different in vitro techniques to characterize the surface-active properties of peptide and peptoid mimics of surfactant protein B in a lipid film: quasi-equilibrium measurement of Π-A isotherms on a LWSB, FM imaging of the surfactant film morphology, and both static-bubble adsorption kinetics measurements and dynamic adsorption hysteresis loops of surface tension versus interfacial area obtained with a PBS. While these techniques are all widely used in the characterization of natural LS and synthetic surfactant replacements, how the resulting data correlate with in vivo efficacy is still under active study in the field. Despite this, we are confident of our ability to elucidate useful information by comparing data obtained with these instruments. Rather than attempting to directly relate the in vitro surface activities of the peptoid mimics to their in vivo efficacy, which can be difficult to quantitate, we have compared them to the surface activities of two peptides that have been previously established by in vivo as well as in vitro studies to be good mimics of SP-B (i.e., SP-B$_{1-25}$ [26–30] and KL$_4$ [35–38]).

We find that the simple, amphipathic, helical peptoid oligomers studied here are able to mimic well many aspects of the in vitro surface activities of these two representative SP-B mimics. PBS hysteresis loops reveal that the peptoids attain similar minimum surface tensions as SP-B$_{1-25}$ and KL$_4$, and in fact 1 and 2 are able to reach near-zero surface tension with a smaller extent of film compression than the peptides (the latter is particularly true of 1). On the other hand, the peptoid-based formulations show higher maximum surface tensions by PBS than the peptides. All of the peptoids show early lift-off and a biomimetic kink or plateau in their Π-A isotherms, with 1 and 2 showing substantially more pronounced plateaus, similar to what is seen for natural LS, than SP-B$_{1-25}$ or KL$_4$. The behavior of peptoid 3 on the Langmuir trough is most similar to that of KL$_4$, while on the PBS it behaves very similarly to SP-B$_{1-25}$. FM images reveal film phase morphologies for the peptoids that seem biomimetic at low surface pressure but are intermediate between those observed for lipids alone and lipid/SP-B$_{1-25}$ films at higher values of Π. However, comparisons of the Π-A isotherms and PBS hysteresis loops indicate that 1 and 2 might have more LS-like surface activity than SP-B$_{1-25}$. Clearly, future work needs to focus on establishing the correlation between these in vitro surfactant characterizations, as well as surface phase morphology and in vivo efficacy. Finally, we note that the relative surface activities of the peptoid oligomers appear to be related to their overall helicity and hydrophobic monomer content, with the most helical and lipophilic peptoid, 1, appearing to mimic the surface activities of natural LS best. Further studies of these peptoid mimics of SP-B will be aimed at elucidating the underlying reasons for these intriguing structure-surface activity relationships.

Recall that natural LS contains two hydrophobic proteins, SP-B and SP-C, both of which are highly conserved across many species [14] and are both thought to be necessary for proper respiratory function [1, 10, 17, 18]. In this study, we have designed helical, facially amphipathic peptoid mimics of SP-B$_{1-25}$ and, through detailed in vitro characterization, shown their potential for use in an exogenous surfactant replacement. In previously published work, we have shown that a helical, longitudinally amphipathic peptoid 22-mer is able to mimic the surface-active behaviors of SP-C [47]. SP-B and SP-C are both helical, amphipathic proteins; however, there are several structural features that distinguish them from one another. In particular, SP-B is facially amphipathic and soluble in aqueous media, while SP-C is longitudinally amphipathic and organosoluble

only. Based on the conservation of both SP-B and SP-C across species, functional mimics of both peptides will likely be needed for the creation of a fully functional, biomimetic LS replacement. We plan to continue with our studies of these peptoid mimics by not only further investigating the necessary structural features for their optimization, but also studying formulations containing peptoid mimics of both SP-B and SP-C.

Significance

We have created three different helical, amphipathic peptoid oligomers that, despite their relatively simple sequences, are able to mimic and perhaps even improve upon the biophysical functioning of the SP-B$_{1-25}$ peptide and KL$_4$, which have been shown by others to be useful as additives to a biomimetic LS replacement. The peptoids were designed to have helical, amphiphilic structures similar to SP-B$_{1-25}$. Characterization of the surface-active behaviors of these SP-B mimics with a variety of experimental tools reveals that the lipid/peptoid films have properties that in many ways are similar to those of lipid/SP-B$_{1-25}$ and lipid/KL$_4$ films. While the correlation between the results of these types of in vitro characterizations of biomimetic LS replacements and their in vivo efficacy is only partially understood, careful comparison of the surface-active behaviors of the peptoids with known SP-B mimics is one way to determine their potential for bioactivity. The interesting correlations we have found between peptoid helical structure, lipophilicity, and surface activity will be studied further. An entirely synthetic, biomimetic formulation containing helical peptoids could potentially fulfill a clinical need for a safe, bioavailable, and inexpensive LS replacement for the treatment of respiratory distress syndrome. Some of the many advantages of using peptoids in therapeutic formulations are the ability of peptoids to form stable helical secondary structure and resist aggregation, their stability to protease degradation, low cost, and relatively simple synthesis. The ability of these simple, helical peptoids to mimic the behavior of SP-B in a lipid environment indicates that they have the potential for broad application in therapeutic formulations that depend on surface-active behavior and lipid/protein interactions.

Experimental Procedures

Materials

Peptide and peptoid synthesis reagents were purchased from Applied Biosystems (Foster City, CA) or Aldrich (Milwaukee, WI). Resins, Fmoc-protected amino acids, and (t-Boc)$_2$O were purchased from NovaBiochem (San Diego, CA), and primary amines were purchased from Aldrich. Solvents for HPLC were purchased from Fisher Scientific (Pittsburgh, PA). DPPC and POPG were purchased from Avanti Polar Lipids (Alabaster, AL), PA was purchased from Aldrich, and Texas red-DHPE was purchased from Molecular Probes (Eugene, OR). All chemicals were used without further purification.

Peptide and Peptoid Synthesis

The modified SP-B$_{1-25}$ peptide and KL$_4$ (Table 1) were synthesized by Fmoc chemistry on solid support (preloaded Wang resin) using an ABI 433A automated peptide synthesizer (Applied Biosystems). Peptoids were also synthesized using the ABI 433A on Rink amide

resin following a submonomer protocol [43], with Boc protection of the *N*Lys side chain [69]. Peptide and peptoid oligomers were cleaved from the resin with a mixture of 95% TFA/water along with necessary protecting group scavengers. Molecules were purified by RP-HPLC using a linear gradient of 20%–95% solvent B in solvent A over 50 min (solvent A is 0.1% TFA in water [v/v], and solvent B is 0.1% TFA in acetonitrile [v/v]). Final purities of the molecules were confirmed to be >97% by analytical RP-HPLC, and molecular weights were confirmed by electrospray mass spectrometry.

Sample Preparation

DPPC, POPG, and PA were each individually dissolved to a known concentration in a 3:1 solution of chloroform and methanol. DPPC, POPG, and PA were combined at a ratio of 68:22:9 (by weight) to a concentration of ~2 mg/ml. This lipid formulation has previously been shown to be a good mimic of the nonprotein fraction of LS [55]. For CD studies in liposomes, lipids were dried under nitrogen and suspended in 4 mM TRIS buffer by sonication at 50°C for ~60 min to a final lipid concentration of 2 mM. For surface activity studies, peptide or peptoid was added to the lipid mixture at 2.16 mol% (corresponding to 10 wt% of SP-B$_{1-25}$) to a final concentration of ~1 mg lipid/ml.

Circular Dichroism

CD spectroscopy studies were performed at room temperature in water, methanol, and a liposome formulation (DPPC:POPG:PA 68:22:9 by weight). Peptide and peptoid samples were prepared in water, methanol, or lipids (1 mM) and buffer (2 mM) to a final concentration of ~60 μM. CD was performed on a Jasco J-715 instrument using a cylindrical quartz cuvette (Hellma, Plainview, BY) with a 0.02 cm path length at room temperature. Each spectrum represents the average of 40 accumulations.

Langmuir-Wilhelmy Surface Balance Studies

Our home-built Langmuir-Wilhelmy surface balance, based on a previously designed system [25], consists of a Langmuir trough fabricated from a solid piece of Teflon and epoxied to a copper plate. Two Teflon barriers are located at opposite ends of the trough and are controlled by a Unislide assembly (Velmex, Bloomfield, NY) with a Silvermax motor (Quicksilver Controls, Covina, CA) to adjust the surface area. Both barriers are spring loaded against the trough to prevent surfactant leakage at surface tensions up to 72 mN/m. The subphase temperature is measured via a thermistor and controlled by 12 thermoelectric couples (Marlow Industries, Dallas, TX) that are connected in series and located between two copper plates. Continuous surface pressure measurements are obtained by a Wilhemy plate transducer controlled by a feedback loop (R&K, Berlin, Germany). The barrier control, temperature control, and pressure transducer are all interfaced with a computer to record experimental data.

For the experiments, the trough was filled with ~300 ml buffer (150 mM NaCl, 5 mM CaCl$_2$, 10 mM HEPES [pH 6.9]) and heated to either 25°C or 37°C. A heated cover plate was used to limit evaporation. The sample, dissolved in a mixture of 3:1 chloroform and methanol, was spread with a syringe at the air/liquid interface and allowed to evaporate for 10 min. The barriers were cycled at 30 mm/min. The film was compressed to near collapse, expanded, and then compressed again. All trough experiments were repeated six times.

Fluorescence Microscopy

In order to obtain fluorescence microscopy images, a Nikon MM40 compact microscope stand with a 100W mercury lamp (Tokyo, Japan) was used in conjunction with the Langmuir trough. The fluorescence was detected by a Dage-MTI three-chip color camera (Dage-MTI, Michigan City, IN) in conjunction with a generation II intensifier (Fryer, Huntley, IL). Samples were spiked with 1 mol% of a fluorescently labeled lipid, Texas red-DHPE, for detection. Previous studies have shown that inclusion of the labeled lipid at this concentration does not alter the surfactant film morphology [70]. Experiments were performed on a buffered subphase at 37°C with

a barrier speed of 2–10 mm/min and were repeated three times for each sample.

Pulsating Bubble Surfactometry

A pulsating bubble surfactometer (General Transco, Largo, FL) was used to obtain both static and dynamic adsorption data. Lipid, lipid/peptide, and lipid/peptoid samples were dried from chloroform/methanol using a DNA 120 speedvac (Thermo Electron, Holbrook, NY), forming a pellet. The pellet was suspended in buffer (150 mM NaCl, 5 mM CaCl$_2$, 10 mM HEPES [pH 6.9]) to 1.0 mg lipid/ml, with a final volume of ~70 μl. Samples were mixed with a pipette, sonicated with a Fisher Model 60 probe sonicator, and then mixed with a pipette again to form a uniform solution. Samples were loaded into a sample chamber with putty placed on the capillary end of the sample chamber; the putty was removed before experiments were performed. A similar method has previously been shown to prevent sample leakage into the capillary [71]. All PBS experiments were performed at 37°C. Static adsorption data were collected for 20 min at a bubble radius of 0.4 mm. Dynamic adsorption data were obtained at a frequency of 20 cycles/min for 20 min following static adsorption, cycling between bubble radii of 0.4 mm and 0.55 mm. All PBS experiments were repeated six times.

Supplemental Data

Supplemental Data are available at http://www.chembiol.com/cgi/content/full/12/1/77/DC1/.

Reference

1. Notter, R.H. (2000). Lung Surfactants: Basic Science and Clinical Applications, Volume 149 (New York: Marcel Dekker).
2. Jobe, A.H. (1993). Drug-therapy: Pulmonary surfactant therapy. N. Engl. J. Med. *328*, 861–868.
3. Greenspan, J.S., Shaffer, T.H., Fox, W.W., and Spitzer, A.R. (1998). Assisted ventilation: physiological implications and complications. In Fetal and Neonatal Physiology,, R.A. Polin and W.W. Fox, eds. (Philadelphia: W.B. Saunders), pp. 1193–1212.
4. Possmayer, F. (1998). Physicochemical aspects of pulmonary surfactant. In Fetal and Neonatal Physiology, R.A. Polin and W.W. Fox, eds. (Philadelphia: W.B. Saunders), pp. 1259–1275.
5. Vangolde, L.M.G., Batenburg, J.J., and Robertson, B. (1988). The pulmonary surfactant system: biochemical aspects and functional significance. Physiol. Rev. *68*, 374–455.
6. Robertson, B., Johansson, J., and Curstedt, T. (2000). Synthetic surfactants to treat neonatal lung disease. Mol. Med. Today *6*, 119–124.
7. Wu, C.W., and Barron, A.E. (2002). Biomimetic lung surfactant replacements. In Biomimetic Materials and Design: Interactive Biointerfacial Strategies, Tissue Engineering, and Drug Delivery, A.K. Dillow and A. Lowman, eds. (New York: Marcel-Dekker Publishers), pp. 565–633.
8. Taeusch, H.W., Lu, K., and Ramierez-Schrempp, D. (2002). Improving pulmonary surfactants. Acta Pharmacol. Sin. *23*, 11–15.
9. Long, W. (1993). Synthetic surfactant. Semin. Perinatol. *17*, 275–284.
10. Goerke, J., and Clements, J.A. (1986). Alveolar surface tension and lung surfactant. In Handbook of Physiology, Section 3: The Respiratory System, Volume 3, Mechanics of Breathing: Part I, A. Fishman, P. Macklem, J. Mead, and S. Geiger, eds. (Bethesda, MD: American Physiological Society), pp. 247–262.
11. Notter, R.H., and Wang, Z. (1997). Pulmonary surfactant: physical chemistry, physiology, and replacement. Rev. Chem. Eng. *13*, 1–118.
12. Possmayer, F., Yu, S.H., Weber, J.M., and Harding, P.G.R. (1984). Pulmonary surfactant. Can. J. Biochem. Cell Biol. *62*, 1121–1133.
13. Goerke, J. (1998). Pulmonary surfactant: functions and molecular composition. Biochim. Biophys. Acta *1408*, 79–89.
14. McCabe, A.J., Wilcox, D.T., Holm, B.A., and Glick, P.L. (2000). Surfactant: a review for pediatric surgeons. J. Pediatr. Surg. *35*, 1687–1700.
15. Creuwels, L.A., van Golde, L.M., and Haagsman, H.P. (1997). The pulmonary surfactant system: Biochemical and clinical aspects. Lung *175*, 1–39.
16. Veldhuizen, R., Nag, K., Orgeig, S., and Possmayer, F. (1998). The role of lipids in pulmonary surfactant. Biochim. Biophys. Acta *1408*, 90–108.
17. Hall, S.B., Venkitaraman, A.R., Whitsett, J.A., Holm, B.A., and Notter, R.H. (1992). Importance of hydrophobic apoproteins as constituents of clinical exogenous surfactants. Am. Rev. Respir. Dis. *145*, 24–30.
18. Wang, Z., Hall, S.B., and Notter, R.H. (1996). Roles of different hydrophobic constituents in the adsorption of pulmonary surfactant. J. Lipid Res. *37*, 790–798.
19. Baatz, J.E., Zou, Y., Cox, J.T., Wang, Z.D., and Notter, R.H. (2001). High-yield purification of lung surfactant proteins SP-B and SP-C and the effects on surface activity. Protein Expr. Purif. *23*, 180–190.
20. Curstedt, T., Johansson, J., Barros-Soderling, J., Robertson, B., Nilsson, G., Westberg, M., and Jornvall, H. (1988). Low-molecular weight surfactant protein type 1: the primary structure of a hydrophobic 8-kDa polypeptide with eight half-cystine residues. Eur. J. Biochem. *172*, 521–525.
21. Hawgood, S., Derrick, M., and Poulain, F. (1998). Structure and properties of surfactant protein B. Biochim. Biophys. Acta *1408*, 150–160.
22. Glasser, S.W., Burhans, M.S., Korfhagen, T.R., Na, C.-L., Sly, P.D., Ross, G.F., Ikegami, M., and Whitsett, J.A. (2001). Altered stability of pulmonary surfactant in SP-C-deficient mice. Proc. Natl. Acad. Sci. USA *98*, 6366–6371.
23. Johansson, J., Curstedt, T., and Jornvall, H. (1991). Surfactant protein B: disulfide bridges, structural properties, and kringle similarities. Biochemistry *30*, 6917–6921.
24. Perez-Gil, J. (2001). Lipid-protein interactions of hydrophobic proteins SP-B and SP-C in lung surfactant assembly and dynamics. Pediatr. Pathol. Mol. Med. *20*, 445–469.
25. Lipp, M.M., Lee, K.Y.C., Waring, A., and Zasadzinski, J.A. (1997). Fluorescence, polarized fluorescence, and Brewster angle microscopy of palmitic acid and lung surfactant protein B monolayers. Biophys. J. *72*, 2783–2804.
26. Longo, M.L., Bisagno, A.M., Zasadzinski, J.A.N., Bruni, R., and Waring, A.J. (1993). A function of lung surfactant protein Sp-B. Science *261*, 453–456.
27. Bruni, R., Taeusch, H.W., and Waring, A.J. (1991). Surfactant protein B: Lipid interactions of synthetic peptides representing the amino-terminal amphipathic domain. Proc. Natl. Acad. Sci. USA *88*, 7451–7455.
28. Baatz, J.E., Sarin, V., Absolom, D.R., Baxter, C., and Whitsett, J.A. (1991). Effects of surfactant-associated protein Sp-B synthetic analogs on the structure and surface-activity of model membrane bilayers. Chem. Phys. Lipids *60*, 163–178.
29. Waring, A., Taeusch, H.W., Bruni, R., Amirkhanian, J., Fan, B.C.R., Stevens, R., and Young, J. (1989). Synthetic amphipathic sequences of surfactant protein B mimic several physiochemical and in vivo properties of native pulmonary surfactant proteins. Pept. Res. *2*, 308–313.
30. Revak, S.D., Merritt, T.A., Hallman, M., Heldt, G., Lapolla, R.J.,

Hoey, K., Houghten, R.A., and Cochrane, C.G. (1991). The use of synthetic peptides in the formation of biophysically and biologically-active pulmonary surfactants. Pediatr. Res. *29*, 460–465.

31. Gordon, L.M., Lee, K.Y.C., Lipp, M.M., Zasadzinski, J.A., Walther, F.J., Sherman, M.A., and Waring, A.J. (2000). Conformational mapping of the N-terminal segment of surfactant protein B in lipid using C-13-enhanced Fourier transform infrared spectroscopy. J. Pept. Res. *55*, 330–347.

32. Kurutz, J.W., and Lee, K.Y.C. (2002). NMR structure of lung surfactant peptide SP-B11–25. Biochemistry *41*, 9627–9636.

33. Cochrane, C.G., and Revak, S.D. (1991). Pulmonary surfactant protein B: structure-function relationships. Science *254*, 566–568.

34. Walther, F.J., Hernandez-Juvel, J., Bruni, R., and Waring, A. (1998). Protein composition of synthetic surfactant affects gas exchange in surfactant-deficient rats. Pediatr. Res. *43*, 666–673.

35. Walther, F.J., Hernandez-Juvel, J.M., Bruni, R., and Waring, A.J. (1997). Spiking Survanta with synthetic surfactant peptides improves oxygenation in surfactant-deficient rats. Am. J. Respir. Crit. Care Med. *156*, 855–861.

36. Revak, S.D., Merritt, T.A., Cochrane, C.G., Heldt, G.P., Alberts, M.S., Anderson, D.W., and Kheiter, A. (1996). Efficacy of synthetic peptide-containing surfactant in the treatment of respiratory distress syndrome in preterm infant rhesus monkeys. Pediatr. Res. *39*, 715–724.

37. Revak, S.D., Cochrane, C.G., Heldt, G.P., Alberts, M.S., Kheiter, A., and Merritt, T.A. (1995). Efficacy of KI4-surfactant in premature-infant monkeys. Pediatr. Res. *37*, A347–A347.

38. Cochrane, C.G., Revak, S.D., Merritt, T.A., Schraufstatter, I.U., Hoch, R.C., Henderson, C., Andersson, S., Takamori, H., and Oades, Z.G. (1998). Bronchoalveolar lavage with KL4-Surfactant in models of meconium aspiration syndrome. Pediatr. Res. *44*, 705–715.

39. Gellman, S.H. (1998). Foldamers: A manifesto. Acc. Chem. Res. *31*, 173–180.

40. Kirshenbaum, K., Zuckermann, R.N., and Dill, K.A. (1999). Designing polymers that mimic biomolecules. Curr. Opin. Struct. Biol. *9*, 530–535.

41. Patch, J.A., and Barron, A.E. (2002). Mimicry of bioactive peptides via non-natural, sequence-specific peptidomimetic oligomers. Curr. Opin. Chem. Biol. *6*, 872–877.

42. Simon, R.J., Kania, R.S., Zuckermann, R.N., Huebner, V.D., Jewell, D.A., Banville, S., Ng, S., Wang, L., Rosenberg, S., Marlowe, C.K., et al. (1992). Peptoids: a modular approach to drug discovery. Proc. Natl. Acad. Sci. USA *89*, 9367–9371.

43. Zuckermann, R.N., Kerr, J.M., Kent, S.B.H., and Moos, W.H. (1992). Efficient method for the preparation of peptoids [oligo(N-substituted glycines)] by submonomer solid-phase synthesis. J. Am. Chem. Soc. *114*, 10646–10647.

44. Huang, C.-Y., Uno, T., Murphy, J.E., Lee, S., Hamer, J.D., Escobedo, J.A., Cohen, F.E., Radhakrishnan, R., Dwarki, V., and Zuckermann, R.N. (1998). Lipitoids: novel cationic lipids for cellular delivery of plasmid DNA in vitro. Chem. Biol. *5*, 345–354.

45. Miller, S.M., Simon, R.J., Ng, S., Zuckermann, R.N., Kerr, J.M., and Moos, W.H. (1995). Comparison of the proteolytic susceptibilities of homologous L-amino acid, D-amino acid, and N-substituted glycine peptide and peptoid oligomers. Drug Dev. Res. *35*, 20–32.

46. Sanborn, T.J., Wu, C.W., Zuckerman, R.N., and Barron, A.E. (2002). Extreme stability of helices formed by water-soluble poly-N-substituted glycines (polypeptoids) with alpha-chiral side chains. Biopolymers *63*, 12–20.

47. Wu, C.W., Seurynck, S.L., Lee, K.Y.C., and Barron, A.E. (2003). Helical peptoid mimics of lung surfactant protein C. Chem. Biol. *10*, 1057–1063.

48. Kirshenbaum, K., Barron, A.E., Goldsmith, R.A., Armand, P., Bradley, E.K., Truong, K.T.V., Dill, K.A., and Cohen, F.E. (1998). Sequence-specific polypeptoids: a diverse family of heteropolymers with stable secondary structure. Proc. Natl. Acad. Sci. USA *95*, 4303–4308.

49. Wu, C.W., Sanborn, T.J., Zuckermann, R.N., and Barron, A. (2001). Peptoid oligomers with α-chiral, aromatic side chains: Effects of chain length on secondary structure. J. Am. Chem. Soc. *123*, 2958–2963.

50. Armand, P., Kirshenbaum, K., Goldsmith, R.A., Farr-Jones, S., Barron, A.E., Truong, K.T.V., Dill, K.A., Mierke, D.F., Cohen, F.E., Zuckermann, R.N., et al. (1998). NMR determination fo the major solution conformation of a peptoid pentamer with chiral side chains. Proc. Natl. Acad. Sci. USA *95*, 4309–4314.

51. Wu, C.W., Kirshenbaum, K., Sanborn, T.J., Patch, J.A., Huang, K., Dill, K.A., Zuckermann, R.N., and Barron, A.E. (2003). Structural and spectroscopic studies of peptoid oligomers with alpha-chiral aliphatic side chains. J. Am. Chem. Soc. *125*, 13525–13530.

52. Wu, C.W., Sanborn, T.J., Huang, K., Zuckermann, R.N., and Barron, A. (2001). Peptoid oligomers with α-chiral, aromatic side chains: Sequence requirements for the formation of stable peptoid helices. J. Am. Chem. Soc. *123*, 6778–6784.

53. Patch, J.A., Kirshenbaum, K., Seurynck, S.L., Zuckermann, R.N., and Barron, A.E. (2004). Versatile oligo (N-substituted) glycines: the many roles of peptoids in drug discovery. In Pseudo-Peptides in Drug Discovery, P.E. Nielsen, ed. (Wienheim, Germany: Wiley-VCG Verlag), pp. 6778–6784.

54. Patch, J.A., and Barron, A.E. (2003). Helical peptoid mimics of magainin-2 amide. J. Am. Chem. Soc. *125*, 12092–12093.

55. Tanaka, Y., Takei, T., Aiba, T., Masuda, K., Kiuchi, A., and Fujiwara, T. (1986). Development of synthetic lung surfactants. J. Lipid Res. *27*, 475–485.

56. Gustafsson, M., Vandenbussche, G., Curstedt, T., Ruysschaert, J.M., and Johansson, J. (1996). The 21-residue surfactant peptide (LysLeu4)4Lys(KL4) is a transmembrane alpha-helix with a mixed nonpolar/polar surface. FEBS Lett. *384*, 185–188.

57. Takamoto, D.Y., Lipp, M.M., Nahmen, A.V., Lee, K.Y.C., Waring, A.J., and Zasadzinski, J.A. (2001). Interaction of lung surfactant proteins with anionic phospholipids. Biophys. J. *81*, 153–169.

58. Lee, K.Y.C., Lipp, M.M., Zasadzinski, J.A., and Waring, A.J. (1997). Effects of lung surfactant specific protein SP-B and model SP-B peptide on lipid monolayers at the air-water interface. Colloids Surf. A: Physiochemical Engin. Aspects *128*, 225–242.

59. Lipp, M.M., Lee, K.Y.C., Takamoto, D.Y., Zasadzinski, J.A., and Waring, A.J. (1998). Coexistence of buckled and flat monolayers. Phys. Rev. Lett. *81*, 1650–1653.

60. Schürch, S., Green, F.H.Y., and Bachofen, H. (1998). Formation and structure of surface film: Captive bubble surfactometry. Biochim. Biophys. Acta *1408*, 180–202.

61. Cai, P., Flach, C.R., and Mendelsohn, R. (2003). An infrared reflection-absorption spectroscopy study of the secondary structure in (KL4)4K, a therapeutic agent for respiratory distress syndrome, in aqueous monolayers with phospholipids. Biochemistry *42*, 9446–9452.

62. Flach, C.R., Cai, P., Dieudonne, D., Brauner, J.W., Keough, K.M.W., Stewart, J., and Mendelsohn, R. (2003). Location of structural transitions in an isotopically labeled lung surfactant SP-B peptide by IRRAS. Biophys. J. *85*, 340–349.

63. Lipp, M.M., Lee, K.Y.C., Zasadzinski, J.A., and Waring, A.J. (1997). Protein and lipid interactions in lung surfactant monolayers. Prog. Colloid Polym. Sci. *103*, 268–279.

64. Cruz, A., Worthman, L.A., Serrano, A.G., Casals, C., Keough, K.M.W., and Perez-Gil, J. (2000). Microstructure and dynamic surface properties of surfactant protein SP-B/dipalmitoylphosphatidylcholine interfacial films spread from lipid-protein bilayers. Eur. Biophys. J. *29*, 204–213.

65. Gupta, M., Hernandez-Juviel, J.M., Waring, A.J., Bruni, R., and Walther, F.J. (2000). Comparison of functional efficacy of surfactant protein B analogs in lavaged rats. Eur. Respir. J. *16*, 1129–1133.

66. Gupta, M., Hernandez-Juviel, J.M., Waring, A.J., and Walther, F.J. (2001). Function and inhibition sensitivity of the N-terminal segment of surfactant protein B (SP-B1–25) in preterm rabbits. Thorax *56*, 871–876.

67. Enhorning, G. (1977). Pulsating bubble technique for evaluating pulmonary surfactant. J. Appl. Physiol. *43*, 198–203.

68. Ingenito, E.P., Morris, L.M.J., Espinosa, F.F., Kamm, R.D., and Johnson, M. (1999). Biophysical characterization and modeling of lung surfactant components. J. Appl. Physiol. *86*, 1702–1714.

69. Krapcho, A.P., and Kuell, C.S. (1990). Mono-protected di-amines: N-tert-butoxycarbonyl-alpha,omega—alkanediamines from alpha,omega-alkanediamines. Synth. Commun. *20*, 2559–2564.

70. Bringezu, F., Ding, J., Berezesinski, G., and Zasadzinski, J.A. (2001). Changes in model lung surfactant monolayers induced by palmitic acid. Langmuir *17*, 4641–4648.

71. Putz, G., Goerke, J., Taeusch, H.W., and Clements, J.A. (1994). Comparison of captive and pulsating bubble surfactometers with use of lung surfactants. J. Appl. Physiol. *76*, 1425–1431.